Many-Body Orbital Paramagnetism in Doped Graphene Sheets

A. Principi and Marco Polini*

NEST, Istituto Nanoscienze-CNR and Scuola Normale Superiore, I-56126 Pisa, Italy

G. Vignale

Department of Physics and Astronomy, University of Missouri, Columbia, Missouri 65211, USA

M. I. Katsnelson

Radboud University Nijmegen, Institute for Molecules and Materials, NL-6525 AJ Nijmegen, The Netherlands

The orbital magnetic susceptibility of a gas of noninteracting massless Dirac fermions is zero when the Fermi energy is away from the Dirac point. Making use of diagrammatic perturbation theory, we calculate exactly the orbital magnetic susceptibility of massless Dirac fermions to first order in the Coulomb interaction demonstrating that it is finite and positive. Doped graphene sheets are thus unique systems in which the orbital magnetic susceptibility is completely controlled by many-body effects.

Introduction.—The diamagnetic properties of carbon allotropes such as diamond and graphite have always attracted a great deal of interest. Early on, it was shown experimentally that the diamagnetic susceptibility of graphite is large and strongly anisotropic [1]. These studies stimulated an intense theoretical activity [2]. The recent isolation of graphene (see Ref. [3] for reviews) has revitalized an interest in the magnetic properties of carbon-based materials. Graphene is a truly two-dimensional (2D) system composed of carbon atoms tightly packed in a honeycomb lattice. States near the Fermi energy of a graphene sheet are described by a massless Dirac equation which has chiral states in which the honeycomb-sublattice pseudospin is aligned either parallel to or opposite to momentum [3]. McClure was the first one to realize that the Landau quantization for 2D massless Dirac fermions (MDFs) in a magnetic field perpendicular to the layer is very special (existence of a zero-energy Landau level) and to conjecture that this is the cause of the large diamagnetic susceptibility of graphite [2,3].

More precisely, McClure showed that the orbital magnetic susceptibility (OMS) of a noninteracting gas of 2D MDFs at a finite temperature T is given by [2,4–7]

$$\chi_{\text{orb}}^{(0)} = -\frac{g_s g_v}{24\pi}\frac{e^2 v^2}{c^2}\frac{1}{k_B T \cosh^2[\mu/(2k_B T)]}$$
$$\overset{T \to 0}{=} -\frac{g_s g_v}{6\pi}\frac{e^2 v^2}{c^2}\delta(\varepsilon_F), \tag{1}$$

where $g_s = g_v = 2$ are spin and valley degeneracies factors, v is the Fermi velocity (which is independent on carrier density), c is the speed of light, μ is the chemical potential, and $\varepsilon_F = \mu(T = 0)$ is the Fermi energy. The zero-temperature OMS of graphene is thus infinite in the undoped limit, i.e., in the limit of zero carrier density. The second line of Eq. (1) encodes another astonishing result [5,6]. The OMS of graphene is exactly zero (at $T = 0$) if

the Fermi energy is away from the Dirac point, i.e., if the system is doped. This situation seems to be really unique.

Equation (1) (and all the other studies [7] of the orbital properties of MDFs we are aware of) heavily relies on a single-particle picture. The fundamental question we address in this Letter is the impact of electron-electron interactions on the OMS of a doped graphene sheet. Short-range repulsive interactions in a neutral Fermi gas [8,9], for example, or Coulomb interactions in an ordinary parabolic-band electron gas [10] enhance the paramagnetic nature of the spin response (eventually driving the system toward a ferromagnetic instability [9,10]) but are typically never strong enough to switch the sign of the orbital response from diamagnetic to paramagnetic. Orbital paramagnetism (OP), although possible in principle, is indeed a rare phenomenon in metals and semiconductors. For example, it has been shown that a 2D electron gas in a periodic potential exhibits OP when the Fermi level is sufficiently close to a saddle point of the band structure [11]. Electrons in the proximity to a superconductor have been shown [12] to exhibit OP. Using diagrammatic perturbation theory up to first order in the Coulomb interaction, we will demonstrate that the OMS of an interacting gas of 2D MDFs is finite and positive. Weakly interacting doped graphene sheets thus represent unique systems with a paramagnetic orbital response of purely many-body origin.

MDF model Hamiltonian and linear-response theory.— The (single-channel) Hamiltonian of a 2D gas of MDFs in the eigenstate representation is ($\hbar = 1$)

$$\hat{\mathcal{H}} = \sum_{k,\lambda}\varepsilon_{k,\lambda}\hat{c}_{k,\lambda}^\dagger\hat{c}_{k,\lambda} + \frac{1}{2S}\sum_{q\neq0}v_q\hat{\rho}_q\hat{\rho}_{-q}, \tag{2}$$

where $\varepsilon_{k,\lambda} = \lambda v k$ ($\lambda = \pm$) are band energies, S is the area of the system, $\hat{\rho}_q = \sum_{k,\lambda,\mu}M_{\lambda\mu}(k,q)\hat{c}_{k-q/2,\lambda}^\dagger\hat{c}_{k+q/2,\mu}$ is the density operator, $v_q = 2\pi e^2/(\epsilon q)$ is the 2D Fourier

transform of the Coulomb potential, ϵ is an average dielectric constant, and $M_{\lambda\mu}(\boldsymbol{k}, \boldsymbol{q})$ are matrix elements which can be found, for example, in Ref. [6]. The many-body properties of doped graphene sheets depend [3,13] on the dimensionless coupling constant (restoring $\hbar$ for a moment) $\alpha_{ee} = e^2/(\epsilon\hbar v)$, which can be tuned experimentally by changing the dielectric environment surrounding the graphene flake [14]. The model (2) requires the introduction of an ultraviolet cutoff $k_{\max}$ [13] on the $\boldsymbol{k}$ sums. This must be done with great care, since, as discussed in Ref. [6], the presence of $k_{\max}$ breaks gauge invariance, which must be restored in the calculations.

The OMS of the system described by $\hat{\mathcal{H}}$, χ_{orb}, can be calculated from [10]

$$\chi_{\mathrm{orb}} = -\frac{e^2}{c^2}\lim_{q\to 0}\frac{\chi(q)}{q^2}, \tag{3}$$

where $\chi(q)$ is a shorthand notation for the static transverse current response function. The bare current-density operator $\hat{\boldsymbol{j}}_{\boldsymbol{q}}$ for MDFs is proportional to the pseudospin-density operator [3]: $\hat{\boldsymbol{j}}_{\boldsymbol{q}} = v\hat{\boldsymbol{\sigma}}_{\boldsymbol{q}}$. In what follows we will calculate $\chi(q)$ up to order q^2 in the long-wavelength $q \to 0$ limit using many-body diagrammatic perturbation theory.

Diagrammatic perturbation theory.—Figure 1 shows the four diagrams that contribute to the transverse ($\boldsymbol{q} = q\hat{\boldsymbol{y}}$) pseudospin response function $\chi(q)$ to first order in the electron-electron interactions. Solid lines are noninteracting Green's functions in the eigenstate representation, $G_\lambda(\boldsymbol{k}, \omega) = [\omega - \varepsilon_{k,\lambda} + i\eta_{k,\lambda}]^{-1}$ where $\eta_{k,\lambda} = \eta\lambda\,\mathrm{sgn}(k - k_{F,\lambda})$, with $\eta = 0^+$. Dashed lines are electron-electron interactions. Here $k_{F,+} = k_F = \sqrt{4\pi n/(g_s g_v)}$ is the Fermi wave number corresponding to an electron concentration n [15] and $k_{F,-} = k_{\max}$.

In the static limit the zeroth-order bare-bubble diagram in panel (a) gives $\chi^{(0)}(q \to 0) = a_0 + a_2 q^2$, with $a_0 =$

$-k_{\max}/(4\pi v)$ and $a_2 = 0$. As discussed in Ref. [6], the term $O(q^0)$ has to be subtracted away to restore gauge invariance. The fact that $a_2 = 0$ originates from a perfect cancellation of intra- and interband contributions. After the *ad hoc* regularization $a_0 \equiv 0$, we find, in agreement with the second line of Eq. (1), that the OMS of the doped noninteracting system is zero: $\chi_{\mathrm{orb}}^{(0)} = 0$.

Panels (b), (c), and (d) in Fig. 1 show the remaining first-order diagrams: panel (b) is the so-called vertex correction, while panels (c) and (d) contain two "self-energy" insertions. The evaluation of these diagrams up to order q^2 is lengthy and will be presented elsewhere. To achieve analytical progress it turns out to be particularly useful [16] to decompose the isotropic interaction $v_{\boldsymbol{k}-\boldsymbol{k}'}$ in Eq. (2) in angular momentum components as $v_{\boldsymbol{k}-\boldsymbol{k}'} = \sum_m V_m(k, k')e^{im(\varphi_k - \varphi_{k'})}$ with $\varphi_k = \hat{\boldsymbol{k}}\cdot\hat{\boldsymbol{x}}$ and the pseudopotentials $V_m(k, k')$ defined in Eq. (10) of Ref. [16]. In what follows we will introduce dimensionless variables: wave vectors will all be measured in units of k_F, the pseudopotentials $V_m(k, k')$ in units of $2\pi e^2/(\epsilon k_F)$, and the response function $\chi(q)$ in units of the single-channel MDF density-of-states $\nu(\varepsilon_F) = \varepsilon_F/(2\pi v^2)$, $\varepsilon_F = v k_F$. The ultraviolet cutoff $k_{\max}$ measured in units of k_F will be denoted by $\Lambda = k_{\max}/k_F$.

Modulo terms $O(q^0)$, which, as mentioned above, must be removed by hand to restore gauge invariance [6], the static transverse response function $\chi(q)$ to first order in α_{ee} reads

$$\chi(q) = g_s g_v \alpha_{ee} \nu(\varepsilon_F) q^2 (\Xi_1 + \Xi_2 + \Xi_3), \tag{4}$$

where the three dimensionless coefficients Ξ_n are given by the sum of vertex $\Xi_n^{(\mathrm{VC})}$ and self-energy $\Xi_n^{(\mathrm{SE})}$ contributions, $\Xi_n \equiv \Xi_n^{(\mathrm{VC})} + \Xi_n^{(\mathrm{SE})}$:

$$\Xi_1^{(\mathrm{VC})} = \frac{1}{128}\int_1^\Lambda \frac{dk}{k^2}\int_1^k \frac{dk'}{k'^2}(k^2 + k'^2)[5V_0(k, k') + V_2(k, k')]$$
$$\equiv \int_1^\Lambda dk f_1^{(\mathrm{VC})}(k), \tag{5}$$

$$\Xi_2^{(\mathrm{VC})} = \frac{1}{384}\int_1^\Lambda \frac{dk}{k^2}\{15(1 - k^2)V_0(k, 1) - 3(1 + k^2)V_2(k, 1)$$
$$+ 2k^2\partial_{k'}[8V_0(k, k') + V_2(k, k')]_{k'=1}$$
$$- k^2\partial_{k'}^2[V_0(k, k') - V_2(k, k')]_{k'=1}\}$$
$$\equiv \int_1^\Lambda dk f_2^{(\mathrm{VC})}(k), \tag{6}$$

$$\Xi_3^{(\mathrm{VC})} = -\frac{1}{384}\{3[21V_0(1, 1) - 6V_1(1, 1) - V_2(1, 1)]$$
$$- 2\partial_{k'}[8V_0(k, k') + 7V_1(k, k') - V_2(k, k')]_{k=k'=1}$$
$$+ \partial_{k'}^2[V_0(k, k') + 2V_1(k, k') + V_2(k, k')]_{k=k'=1}\}$$
$$\equiv 2\int_0^\pi d\theta f_3^{(\mathrm{VC})}(\theta), \tag{7}$$
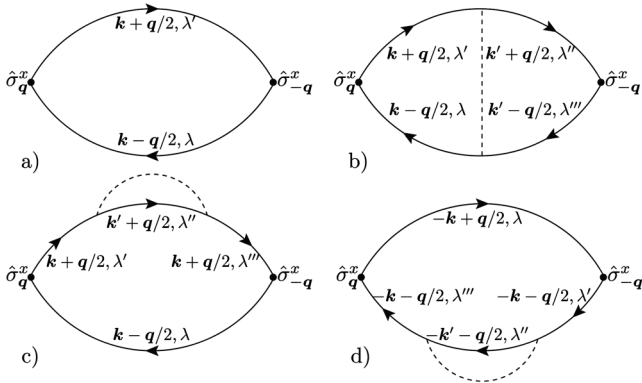

FIG. 1. Diagrams for the orbital magnetic susceptibility. (a) The noninteracting bubble. (b) The first-order vertex correction. (c) and (d) The two first-order self-energy diagrams. The wave-vector labeling of the propagators ensures time-reversal symmetry and thus guarantees that the two self-energy diagrams give an identical contribution.

$$\Xi_1^{(SE)} = \frac{1}{128} \int_1^\Lambda dk \int_1^k dk' \left[5\frac{k^2 + k'^2}{k^2 k'^2} V_0(k,k') - 3\frac{5k^4 + k^2 k'^2 + 5k'^4}{k^3 k'^3} V_1(k,k') + \frac{k^2 + k'^2}{k^2 k'^2} V_2(k,k') + \frac{9}{kk'} V_3(k,k') \right], \quad (8)$$

$$\Xi_2^{(SE)} = \frac{1}{768} \int_1^\Lambda \frac{dk}{k^2} \{ 3(11 - 10k^2) V_0(k,1) + 3k(36k^2 - 5) V_1(k,1) - 3(10k^2 + 1) V_2(k,1) - 81k V_3(k,1) + 30 V_4(k,1)$$
$$- \partial_{k'}[7k^2 V_0(k,k') + 9k(2k^2 + 1) V_1(k,k') - 7k^2 V_2(k,k') + 9k V_3(k,k')]_{k'=1} + k^2 \partial_{k'}^2 [V_0(k,k') - V_2(k,k')]_{k'=1} \}, \quad (9)$$

and

$$\Xi_3^{(SE)} = -\frac{1}{768} \{ 33 V_0(1,1) - 72 V_1(1,1) - 27 V_2(1,1) - 48 V_3(1,1) + 30 V_4(1,1) + \partial_{k'}[7 V_0(k,k') + 23 V_1(k,k') + 5 V_2(k,k')$$
$$+ 5 V_3(k,k') + 16 V_4(k,k')]_{k=k'=1} - \partial_{k'}^2 [4 V_0(k,k') + 8 V_1(k,k') + 2 V_2(k,k') - 4 V_3(k,k') - 2 V_4(k,k')]_{k=k'=1} \}$$
$$\equiv 2 \int_0^\pi d\theta f_3^{(SE)}(\theta). \quad (10)$$

It is easy to prove that $f_1^{(VC)}(k \to \infty) \to 5/(128k) + 5(18C - 7)/(576\pi k^2) + O(k^{-3})$ and that $f_2^{(VC)}(k \to \infty) \to -5/(128k) + O(k^{-3})$. Here $C \simeq 0.916$ is Catalan's constant. This implies that the sum $f_1^{(VC)}(k) + f_2^{(VC)}(k)$ decays like k^{-2} for large k: we can thus take the limit $\Lambda \to \infty$ in Eqs. (5) and (6) finding a finite, cutoff independent result for the sum $\Xi_1^{(VC)} + \Xi_2^{(VC)}$. This property is identically shared by the sum $\Xi_1^{(SE)} + \Xi_2^{(SE)}$. Thus vertex and self-energy contributions are separately convergent in the ultraviolet limit. It is however crucial to take into account both contributions to have a finite result. Indeed, the quantities $\Xi_3^{(VC)}$ and $\Xi_3^{(SE)}$ are separately strongly divergent: for the Coulomb potential we find $f_3^{(VC)}(\theta \to 0) = -f_3^{(SE)}(\theta \to 0) = 1/(192\pi\theta^3)$ at small angles. The subleading terms in the Taylor expansions of $f_3^{(VC)}(\theta)$ and $f_3^{(SE)}(\theta)$ are also singular ($\propto 1/\theta$) but these singularities do not cancel out upon summing $f_3^{(VC)}(\theta)$ with $f_3^{(SE)}(\theta)$ and are an artifact of first-order perturbation theory, which misses screening. These pathologies are commonly cured [10] by using a statically screened Thomas-Fermi interaction: (restoring units for a moment) $v_q = 2\pi e^2/[\epsilon(q + q_{TF})]$, $q_{TF} = g_s g_v \alpha_{ee} k_F$ being the Thomas-Fermi screening wave number [17].

Substituting Eq. (4) into (3) we finally find that the OMS is given by

$$\chi_{orb} = g_s g_v \frac{e^2 v^2}{c^2} \frac{\alpha_{ee} \mathcal{N}(\alpha_{ee})}{\varepsilon_F}, \quad (11)$$

where we have defined $\mathcal{N}(\alpha_{ee}) = -(\Xi_1 + \Xi_2 + \Xi_3)/(2\pi)$. Note that the final result (11) is formally beyond the first order in α_{ee} since Thomas-Fermi screening introduces nonlinear dependencies on α_{ee}. The quantity $\mathcal{N}$ is presented in Fig. 2. One can see, first of all, that the function $\mathcal{N}(\alpha_{ee})$ is positive, which corresponds to OP, and depends weakly on α_{ee}. It is easy to show that $\mathcal{N}(\alpha_{ee} \to 0) \to -\ln(\alpha_{ee})/(48\pi^2)$, implying that $\chi_{orb} \propto -\alpha_{ee} \ln(\alpha_{ee})$ in the weak-coupling limit [18]. Using Eq. (11) for $\alpha_{ee} = 0.9$ and a doping $n = 10^{12} \text{cm}^{-2}$, we find that the OMS per unit mass is approximately $4 \times$

10^{-6} emu/g (to be compared with the one of graphite in absolute value, which is of the order of 10^{-5} emu/g [2]). We remark that the paramagnetic nature of the orbital response, i.e., $\chi_{orb} > 0$, is stable with respect to changes in the range of interparticle interactions. Using the Hamiltonian (2) with contact repulsive interactions of strength v_0 (i.e., $v_q = v_0 > 0$), we find the analytical expression

$$\chi_{orb} = g_s g_v \frac{e^2}{c^2} \frac{13}{256\pi^2} v_0. \quad (12)$$

Discussion and conclusions.—Our findings can be tested experimentally in a variety of ways. The most direct one is to measure the thermodynamic magnetization as a function of an applied magnetic field. Ingenious setups for these types of measurements have already been successfully applied to various carbon structures [19] and to conven-
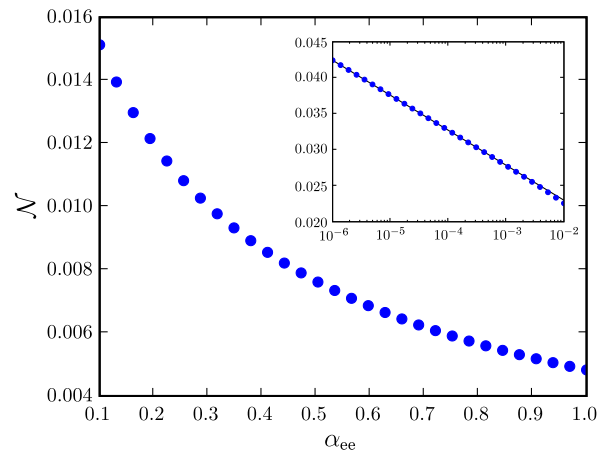

FIG. 2 (color online). The dimensionless quantity $\mathcal{N} = -(\Xi_1 + \Xi_2 + \Xi_3)/(2\pi)$ as a function of the fine-structure constant α_{ee}. Note that $\mathcal{N}(\alpha_{ee}) > 0$ and that it depends weakly on α_{ee}. Inset: a zoom for very small α_{ee}. The horizontal axis is in logarithmic scale. The solid line represents the analytical weak-coupling result, $\mathcal{N}(\alpha_{ee} \to 0) \to -\ln(\alpha_{ee})/(48\pi^2)$.

PHYSICAL REVIEW LETTERS

tional 2D electron gases [20]. Spin and orbital responses can be distinguished by applying a tilted magnetic field [21]. To enhance the magnetic response one can resort to graphene laminate [22] (actually, the first magnetic measurements in this system have already been done [23]). Another possibility is to use macroscopically large graphene films from carbon on copper foil, as demonstrated in Ref. [24].

Interestingly, OP in doped graphene can be probed also by acoustic measurements. Indeed, mechanical deformations of graphene are known to produce a pseudomagnetic gauge field [25]. The induced vector potential $A(r)$ is proportional to the deformation tensor $u_{ij}(r)$ and the pseudomagnetic field is given by the usual relation $B_S(r) = \nabla_r \times A(r)$. Using the basic equations of the theory of elasticity, it is easy to prove that the coupling between deformations and electronic degrees of freedom, which occurs via $A(r)$, leads to a renormalization of the shear modulus $\mu_s \rightarrow \mu_s(q) = \mu_s - g_2^2 \chi_{orb} q^2/e^2$ and thus of the transverse sound velocity $\omega^2(q) = \mu_s(q)q^2/\rho$, where g_2 is a coupling constant [26] and ρ is the mass density. The positive sign of χ_{orb} thus implies a softening of the sound velocity with increasing q whereas diamagnetic response would result in the opposite behavior.

In summary, we have shown that doped graphene sheets have a very intriguing orbital magnetic response. If electron-electron interactions are neglected, the OMS is identically zero. When electron-electron interactions are taken into account, the OMS turns out to be finite. To the best of our knowledge, this is the first system we are aware of in which many-body effects control completely the orbital response. The sign of the OMS cannot be predicted *a priori*. To first order in Coulomb interactions we have shown that it is positive. Weakly interacting doped graphene sheets are thus many-body orbital paramagnets.

*m.polini@sns.it; URL: http://qti.sns.it/

[1] K. S. Krishnan, Nature (London) **133**, 174 (1934); N. Ganguli and K. S. Krishnan, Proc. R. Soc. London **177**, 168 (1941).

[2] J. W. McClure, Phys. Rev. **104**, 666 (1956); J. W. McClure, *ibid.* **119**, 606 (1960); M. P. Sharma, L. G. Johnson, and J. W. McClure, Phys. Rev. B **9**, 2467 (1974).

[3] A. K. Geim and K. S. Novoselov, Nature Mater. **6**, 183 (2007); M. I. Katsnelson, Mater. Today **10**, 20 (2007); A. H. Castro Neto *et al.*, Rev. Mod. Phys. **81**, 109 (2009); A. K. Geim, Science **324**, 1530 (2009).

[4] S. A. Safran and F. J. DiSalvo, Phys. Rev. B **20**, 4889 (1979).

[5] M. Koshino and T. Ando, Phys. Rev. B **75**, 235333 (2007); M. Koshino, Y. Arimura, and T. Ando, Phys. Rev. Lett. **102**, 177203 (2009).

[6] A. Principi, M. Polini, and G. Vignale, Phys. Rev. B **80**, 075418 (2009).

[7] S. G. Sharapov, V. P. Gusynin, and H. Beck, Phys. Rev. B **69**, 075104 (2004); A. Ghosal, P. Goswami, and S. Chakravarty, *ibid.* **75**, 115123 (2007); M. Nakamura, *ibid.* **76**, 113301 (2007).

[8] K. H. Huang, *Statistical Mechanics* (John Wiley, New York, 1987).

[9] G.-B. Jo *et al.*, Science **325**, 1521 (2009).

[10] G. F. Giuliani and G. Vignale, *Quantum Theory of the Electron Liquid* (Cambridge University Press, Cambridge, England, 2005).

[11] G. Vignale, Phys. Rev. Lett. **67**, 358 (1991).

[12] C. Bruder and Y. Imry, Phys. Rev. Lett. **80**, 5782 (1998).

[13] Y. Barlas *et al.*, Phys. Rev. Lett. **98**, 236601 (2007); M. Polini *et al.*, Solid State Commun. **143**, 58 (2007).

[14] C. Jang *et al.*, Phys. Rev. Lett. **101**, 146805 (2008); L. A. Ponomarenko *et al.*, *ibid.* **102**, 206603 (2009).

[15] The model's particle-hole symmetry guarantees that electron-doped and hole-doped systems have identical OMS.

[16] G. Borghi *et al.*, Solid State Commun. **149**, 1117 (2009).

[17] M. I. Katsnelson, Phys. Rev. B **74**, 201401(R) (2006).

[18] More sophisticated (i.e., dynamical) treatments of screening [see G. Vignale, M. Rasolt, and D. J. W. Geldart, Phys. Rev. B **37**, 2502 (1988)] are not expected to alter the $\alpha_{ee} \ln(\alpha_{ee})$ functional dependence of χ_{orb} at weak coupling.

[19] J. Heremans, C. H. Olk, and D. T. Morelli, Phys. Rev. B **49**, 15 122 (1994).

[20] O. Prus *et al.*, Phys. Rev. B **67**, 205407 (2003); A. A. Shashkin *et al.*, Phys. Rev. Lett. **96**, 036403 (2006).

[21] F. F. Fang and P. J. Stiles, Phys. Rev. **174**, 823 (1968).

[22] P. Blake *et al.*, Nano Lett. **8**, 1704 (2008); Y. Hernandez *et al.*, Nature Nanotech. **3**, 563 (2008).

[23] M. Sepioni, S. Rablen, R. R. Nair, J. Narayanan, F. Tuna, R. Winpenny, A. K. Geim, and I. V. Grigorieva (to be published).

[24] S. Bae *et al.*, arXiv:0912.5485v3.

[25] F. Guinea, M. I. Katsnelson, and A. K. Geim, Nature Phys. **6**, 30 (2010); M. A. H. Vozmediano, M. I. Katsnelson, and F. Guinea, arXiv:1003.5179v1.

[26] See for example M. Gibertini *et al.*, Phys. Rev. B **81**, 125437 (2010).